**Renewable Energy**
November 2022, Volume 200, Pages 983-995
https://doi.org/10.1016/j.renene.2022.10.006
https://archimer.ifremer.fr/doc/00797/90865/



# Experimental investigation of the influence of mast proximity on rotor loads for horizontal axis tidal turbines

Shoukat G. [1,*], Gaurier Benoît [2], Facq Jean-Valery [2], Payne G.S. [3]

[1] R & D Department, Gavin and Doherty Geosolutions, D14 X627, Ireland
[2] Laboratoire Comportement des Structures en Mer, Ifremer, 62200, France
[3] LHEEA, Ecole Centrale de Nantes and CNRS (UMR6598), 44300, France

* Corresponding author : G. Shoukat, email address : gshoukat@gdgeo.com

Benoit.Gaurier@ifremer.fr ; jean.valery.facq@ifremer.fr ; gregory.payne@farwind-energy.com

**Abstract :**

While the world continues to grapple with the increasingly prominent impact on the planet of climate change, a shift towards greater reliance on renewable energy sources is observed. Wind, hydro and solar have seen a rise in uptake, however, tidal energy represents massive untapped potential. For tidal energy to become economically viable, focus must shift towards designing efficient yet structurally sound designs. The current study investigates the influence of the tower distance from the rotor plane on turbine performance, and on rotor loading. A test scale instrumented tidal stream turbine is studied in a water flume tank at the laboratory of IFREMER in Boulogne-sur-Mer, France. Experiments are carried out with 14 different tower positions and the turbine performance coefficients are compared. Both mean and values remain unaffected for these different positions. However, the structural rotor loading is found to fluctuate significantly as the distance between the tower and rotor is reduced. Load measurements are analysed in terms of coefficient of variation, through frequency analysis, in relation with the azimuthal position of the rotor and finally in terms of exceedance. All the experimental measurements associated with this study are available from: https://doi.org/10.17882/81077.

**Highlights**

► Tidal turbine tower distance to rotor affects blade loads. ► Average loads unaffected but load variability and extreme values change. ► Experimental investigation in a flume tank with different tower positions. ► Tower proximity and rotating effect make loads register at blade passing frequency.

**Keywords** : tidal energy, tidal turbine loading, experimental investigation, tower to rotor proximity

# 1. Nomenclature

## *1.1. Abbreviations*

| | |
|---|---|
| **DoF** | **D**egrees **o**f **F**reedom |
| **CAD** | **C**omputer **A**ided **D**esign |
| $\mathbf{C_p}$ | **C**oefficient **o**f **P**ower |
| $\mathbf{C_t}$ | **C**oefficient **o**f **T**hrust |
| **TSR** | **T**ip **S**peed **R**atio |
| **LDA** | **L**aser **D**opper **A**nemometer |
| **LDV** | **L**aser **D**opper **Velocimeter** |
| **Re** | **Re**ynolds Number |
| **CoV** | **C**oefficient **o**f **V**ariation |
| **FFT** | **F**ast **F**ourier **T**ransformation |
| **TI** | **T**urbulence **I**ntensity |
| **TDC** | **T**op **D**ead **C**enter |
| **TST** | **T**idal **S**tream **T**urbine |
| **LCOE** | **L**evelized **C**ost **o**f **E**nergy |
| **CFD** | **C**omputational **F**luid **D**ynamics |

### 1.2. Symbols

| Symbol | Description | Units |
|---|---|---|
| $\omega$ | Angular frequency | $s^{-1}$ |
| $\sigma$ | Standard deviation | |
| $\mu$ | Mean | |
| $\hat{d}$ | Normalised mast position | |
| $f_0$ | Turbine rotational frequency | Hz |
| $f$ | Frequency | Hz |
| $\bar{f}$ | Normalised frequency | |
| $u$ | Streamwise component of velocity | $m\,s^{-1}$ |
| $\bar{u}$ | Average streamwise component of velocity | $m\,s^{-1}$ |
| $\nu$ | Kinematic viscosity of water | $m^2\,s^{-1}$ |
| $c_{75}$ | Blade chord length at 75% of rotor radius | m |
| $\lambda$ | TSR | |
| $Q$ | Torque | N m |
| $\rho$ | Fluid density | $kg\,m^{-3}$ |
| $A$ | Rotor swept area | $m^2$ |
| $U$ | Stremwise onset flow velocity | $m\,s^{-1}$ |
| $F_{x_1}$ | Flapwise load on blade 1 | N |
| $\bar{F}_{x_1}$ | Mean of flapwise load on blade 1 | N |

## 2. Introduction

An increased focus on renewable energy technology is seen in this decade to achieve the 2030 climate goals. An EU wide push is observed in developing and deploying various onshore and offshore energy capturing devices for electricity production. This includes wind turbines, wave energy converters and tidal turbines. The Ocean Energy Strategic Road map for the European Union estimates that the renewable energy industry could develop into a staggering €653bn by 2050 [1].

Tidal energy is extracted - as the name suggest - from the tidal currents which are energetically dense and offers a high level of predictability on large timescales. Tidal energy, due to its reliability and predictability, holds great potential. Commercial interest in the sector continues to grow. Full scale devices have been developed and deployed at test and commercial sites [2, 3, 4]. Europe is leading the technological development in Tidal Stream Turbines (TSTs) as approximately 50% of the TST developers are within Europe [5] and the European targets are ambitious with the aim of installing 100 GW of wave and tidal capacity by 2050 [6, 7]. The majority of the tidal turbine concepts are based on the horizontal axis configuration [8].

However, for TSTs to develop into a commercially viable technology, they must be designed to withstand the extreme marine conditions without being over engineered. Due to turbulence in waves the structural loading, and the performance of TSTs are impacted by these rapidly evolving unsteady conditions, which in turn influence the fatigue of individual components and hence the lifespan and by extension the energy yield from the turbines. In [9] and [10], using an active grid turbulence generator in a recirculating water tunnel, it is shown that sheared inflows result in a 5 − 10% drop in the maximum power coefficient for a three-bladed tidal turbine model, and an increase of 30 and 50% in torque and thrust fluctuations respectively, when compared to the low turbulent case. The generated turbulence intensities in these studies correspond to what is observed at sea for highly energetic sites. In the Alderney Race (English channel) for instance, the turbulence intensity is estimated to be between 6 and 13% [11], and waves can occasionally reach significant heights of 7 m during storms according to [12]. The bathymetry-generated turbulence associated with this site and its effect on a tidal turbine model is investigated in [13, 14].

Previous experimental work with TSTs has explored their performance under a variety of flow and wave conditions. Spectral analysis for unsteady turbine loading under varying Turbulence Intensity (TI) was studied [15, 16] and the frequencies which contribute towards the different loads experienced by the TST are well documented [17, 18]. The latter study is further expanded to investigate the variation in the power spectra of the flow due to the rotor aero/hydrodynamics and the deceleration of the incident fluid in [19].

Literature on the interaction between the turbine and turbulent flow is quite rich. Investigations into how turbulence affects the rotor loads confirm that at deployment sites where the TI averages between 15% - 20 %, power coefficients fluctuate by about 10 % and that the rotor loads can fluctuate five fold in most extreme cases [20]. Although TSTs have some similarities with wind turbines, significant differences in operational aerodynamics/hydrodynamics exist, for instance, in the onset of cavitation and the interaction with the free surface. Experiments have been carried out for test scale TSTs at different pitch angles and Tip Speed Ratios (TSR) for different onset velocities [21]. This experimental campaign also collects important data on turbine performance under straight and/or yawed flow, on the effect on the performance of the variation in the tip immersion of the rotor, interaction between twin rotors, and the inception of cavitation. In [22], the impact on turbine performance of the unsteady flow experienced at a tidal test site is investigated by comparisons with the performance of the same turbine in the steady flow conditions of a towing tank. That study also looks at the effect of control strategy of the rotor velocity (PID feedback loop versus open-loop control) on the turbine performance. The topic of turbine control is further investigated using experimental scale models in [23] where different levels of stiffness in the speed control loop are explored to analyse their effect on loads due to turbulence and waves. In [24], an advanced turbine scale model is equipped with a mechanism allowing blade pitch control. This turbine is used to implement a control strategy aimed at maintaining power output in time varying flow. This blade pitch control approach is compared with control strategies based on fixed pitch with rotor overspeed and underspeed.

Another study into the interaction between turbulent flow and TST which looked into the wake produced by this interaction showed that for low frequencies, the instantaneous power produced is influenced by the incident turbulent flow. The critical frequency at which the turbine response gets decoupled from the incoming turbulent flow varies linearly with the angular frequency of the rotor [17]. The measurements however, were not taken directly at the rotor or the root of the blades. They were taken from static torque sensors mounted between the stator part of the motor and the turbine structure. In the current study, the sensors are installed in the roots of the blade and the rotor itself to increase accuracy.

The common theme in all these experimental investigations was to determine the influencing factors in the overall cyclic loading which contribute to component fatigue and hence, the lifespan of the turbine which in turn affects the levelised cost of energy of a project.

Researchers have also used numerical approaches to calculate the hydrodynamic loading on TSTs. RANS and LES models were developed and validated against actual test site data. These models were then used to calculate the streamwise and spanwise pressures on the blades [25]. The research further analysed the blockage effect of the tower on the fluctuations in loading on the rotor and the blades. Another numerical study with a similar focus to the current study investigated the impact of different tower diameters on the fluctuation of the loads as the blades passed by the tower [26]. As expected, greater fluctuation was observed when the tower diameter was increased.

While the influence of support structures on horizontal axis wind turbines is fairly well understood and documented [27], this is less true for TSTs. The interaction effects between a tidal turbine rotor and two different support structures have been investigated using CFD in [28]. It shows that the integrated rotor forces are higher in the presence of a cylindrical support structure compared to an elliptical one. The velocity deficit just in front of the support structure is shown to be 20% higher for the cylindrical support structure than for the elliptical one. The impact of the mast on the overall performance of a tidal turbine and on its loading has also been investigated numerically in [29], where different stanchion profile shapes are explored for a fixed distance between the stanchion and the rotor plane. Follow-up numerical investigations (using CFD) are reported in [30] with a stanchion of cylindrical section located at three different distances downstream and upstream of the rotor disc. To the best of authors' knowledge, the influence of mast proximity to the rotor plane has not been researched experimentally and is therefore, the subject of the present study.

The experimental setup including the different testing configurations and flow parameters used in this study are covered in section 3. Section 4 covers the performance characterisation, variation in loading and the analysis drawn from these results. Finally, section 5 concludes this investigation. The raw experimental data on which this study is based is available from: https://doi.org/10.17882/81077.

## 3. Experimental Setup

### *3.1. Turbine Model*

A three-bladed, horizontal axis turbine mounted on the flume bottom was used for these experiments with a rotor diameter of 724 mm. The three blades each have a load sensor at their root measuring the three moments as well as the flapwise and edgewise forces. A CAD image of the turbine used is shown in figure 1. A focus of the turbine design and its instrumentation is to obtain the best possible quality of load measurements. This approach required the sensors to be located as close as possible to the location where the loads are actually being applied. This was ensured by installing the sensors upstream of the rotary seals, hence preventing associated parasitic friction from affecting the measurements. However, this puts the sensors in a wet environment. Therefore, these sensors were made waterproof. The following quantities are analysed in the present study:

- Rotor torque
- Rotor thrust
- Rotational velocity
- Rotor azimuthal position
- Flapwise force on each of the three blades

The turbine mast is 70 mm in diameter and its axis is located 594 mm downstream of the rotor plane. It was bolted to the tank floor. Except when specified otherwise, the signals from all the turbine sensors were sampled at 256 Hz in a synchronous manner and each test run lasted 360 s. More information on the turbine and its instrumentation can be found in [31].

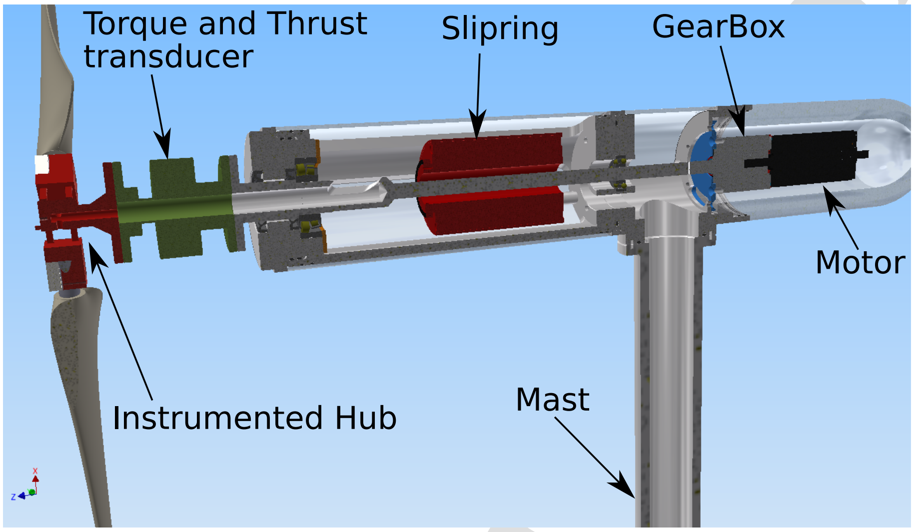


Figure 1: Cross-Sectional View of the Turbine displaying its sensors

### *3.2. Testing Facility*

The tests were carried out in the wave and current recirculating flume tank of IFREMER at Boulogne-sur-mer, France. The flow channel is 4 m in width, 18 m in length and was operated at a depth of 2 m [32]. The turbine is kept at the centre of the tank with reference to the length and width of the tank. The channel-to-turbine blockage ratio came out to be as low as 0.0512, taking into account the rotor, tower and hub. The flume tank is capable of functioning at multiple velocities. For the experiments carried out in this campaign, three different flow velocities were used: $U \in \{0.8, 1.0, 1.2\}\mathrm{m\,s^{-1}}$. The inlet of the flume tank has removable flow conditioning units to alter the turbulence intensity within the tank. For these experiments, a turbulence intensity (considering on the stream-wise velocity component $u$) of $TI_u = 1.5\%$ was used. Without the flow conditioning units, the maximum turbulence can go upto $TI_u = 15\%$. $TI_u$ is given by:

$$TI_u = 100\frac{\sigma(u)}{\bar{u}}$$

where:

- $\sigma(u)$ is the standard deviation recorded for the streamwise incident fluid velocity component $u$.
- $\bar{u}$ is the average of the streamwise incident fluid velocity component $u$.

A more detailed description of the flume tank can be found in [33]. Further measurements were taken to check the spatial variation in the streamwise velocity over the rotor area in the absence of turbine and came out to be less than 4 %. A schematic of the tank is shown in figure 2.

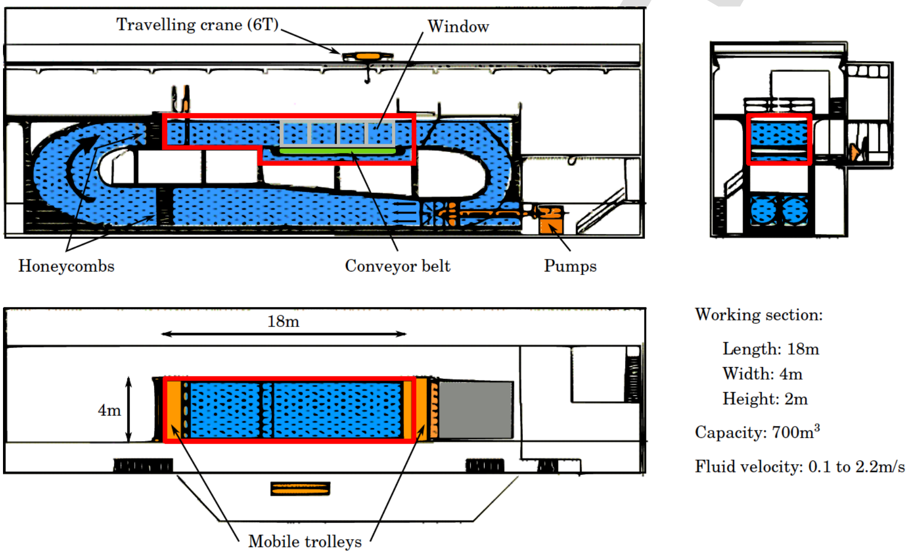


Figure 2: A schematic of the flume tank at Ifremer summarising the dimensions of the tank

A 3D Laser Doppler Velocimetry system (LDV) is used for flow velocity measurements. It is mounted at a distance of four times the rotor diameter upstream of the turbine rotor, aligned with the rotor axis. The system used for the experiments is produced by Dantec Dynamics. This three component LDV system consists of six laser beams arranged in intersecting pairs associated with three different wave lengths - 514 nm, 488 nm, 532 nm. Velocity measurements occur each time a seeding particle crosses the measurement volume created by the crossing laser beams. The sampling rate of the LDV system is therefore nonuniform. An image of the setup in the flume tank is shown in figure 3.

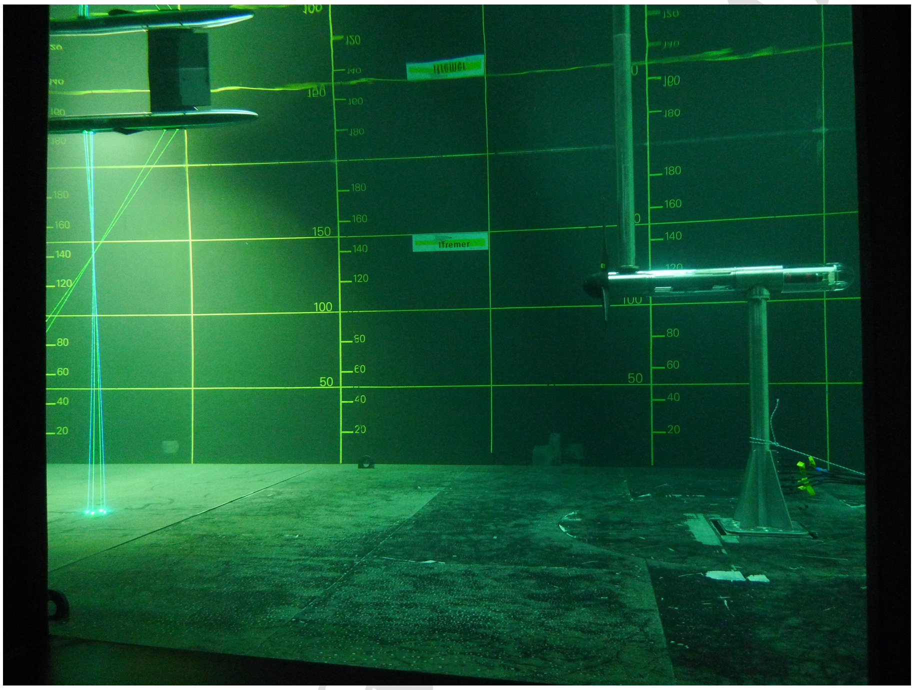

Figure 3: Final setup of the experiment: hexapod (not visible in the picture) holds and moves the dummy mast above the turbine model which is mounted on to the tank floor. To the left, the LDV can be seen in operation

Finally, the last item used to complete the experimental setup was the Stuart Platform (or hexapod) which was used to control the dummy mast position, whose external diameter is the same as the structural mast (70 mm). The Stuart Platform provides six degrees of freedom (DoF) - three translations and three rotations - motion, and allows positioning of the mast at different locations with an accuracy of the order of 0.1 mm. A CAD image of the setup with the Stuart Platform, dummy mast and the turbine in place is presented in figure 4.

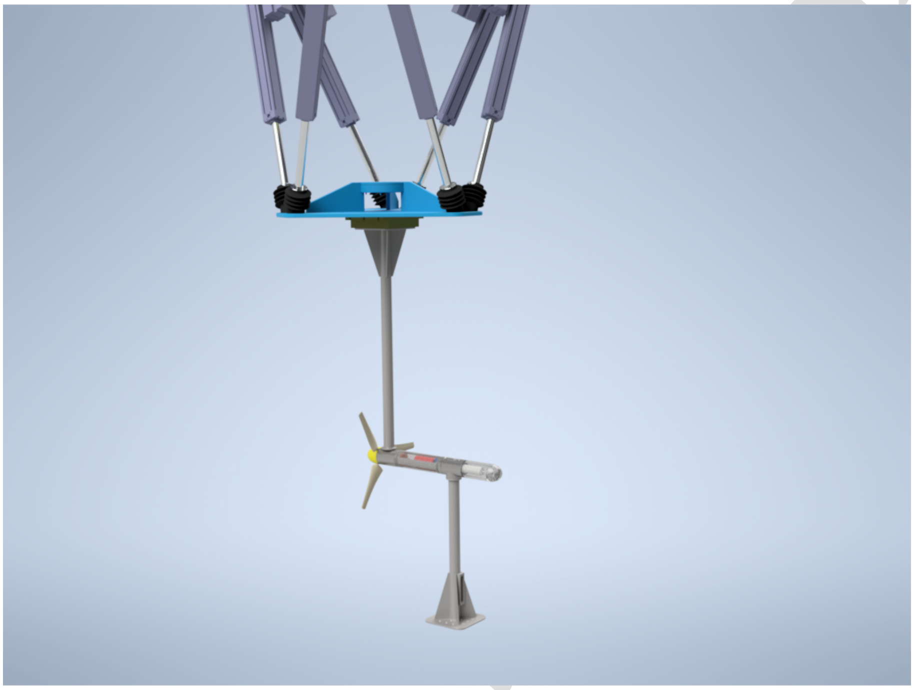

Figure 4: CAD view of the setup with turbine, dummy mast and Stuart Platform. It should be noted that the tank walls and the water free surface are not shown in this representation.

### 3.3. Reynolds number

The chord-based Reynolds numbers at 75% of the blade radius is defined by:

$$Re_{75} = \frac{c_{75}\bar{u}\sqrt{1+(0.75\lambda)^2}}{\nu} \tag{1}$$

where $c_{75}$ is the blade chord length at 75% of the rotor radius, $\lambda$ the TSR and $\nu$ the kinematic viscosity. Table 1 shows values of $Re_{75}$ for different combinations of TSR and onset flow velocity.

## 4. Results and analysis

### 4.1. Performance Coefficients

To characterise the performance of a turbine, non-dimensional parameters are used. The two parameters used in this study are the Coefficient of Power

| $U$ (m s$^{-1}$) \ $\lambda$ | 2 | 4 | 6 |
|---|---|---|---|
| 0.8 | $6.93 \times 10^4$ | $1.21 \times 10^5$ | $1.77 \times 10^5$ |
| 1 | $8.66 \times 10^4$ | $1.52 \times 10^5$ | $2.21 \times 10^5$ |
| 1.2 | $1.04 \times 10^5$ | $1.82 \times 10^5$ | $2.66 \times 10^5$ |

Table 1: $Re_{75}$ values

($C_p$) and the Coefficient of Thrust ($C_t$). $C_p$ provides a measure of the power generated by a turbine whereas $C_t$ indicates the stream-wise loading the rotor is subjected to. They are calculated as per the following equations:

$$C_p = \frac{Q\omega}{\frac{1}{2}\rho A \bar{U^3}} \tag{2}$$

$$C_t = \frac{T}{\frac{1}{2}\rho A \bar{U^2}} \tag{3}$$

where:

$C_p, C_t$ : Non-Dimensionalised coefficients corresponding to power and thrust respectively.
$Q$ : Torque as measured by the sensor in the rotor
$\omega$ : Angular velocity of the rotor
$\rho$ : Fluid density
$A$ : Rotor swept area
$U$ : Streamwise onset flow velocity
It should be noted that the velocity measurements were cubed (for eq. 2) and squared (eq. 3) before averaging, as suggested in [20].

Test configurations associated with three different flow velocities: 0.8 m s$^{-1}$, 1.0 m s$^{-1}$ and 1.2 m s$^{-1}$ and four distances between the rotor plane and the dummy tower: 594 mm, 427 mm, 260 mm and 93 mm, were investigated. The $C_p$ for the three different velocities and the different distances between the rotor and the dummy mast are shown in the figure 5, with the distances normalised by the rotor diameter and denoted $\hat{d}$. While this figure does not provide conclusive information about effect of the dummy mast position on $C_p$, it does show the impact of $Re$ on the evolution of $C_p$.

We observe that as the velocity, and hence $Re$, increases, the maximum $C_p$, taking place around TSR = 4, also increases. However, the rate of increase decreases as we move to higher velocity and the difference in performance decreases. Strictly speaking, it would have been desirable to use a higher $Re$ to make the results Reynolds independent. This would have however led to rotor torque values beyond what the model can cope with.

The steepest rise in $C_p$ is seen between TSR 2 and 3. This steep gradient is believed to be associated with a flow regime transition. The exact TSR of that transition is believed to fluctuate and this could explain the variations in $C_p$ observed at TSR = 2.5 for the $1\,\mathrm{m\,s^{-1}}$ case. This could also explain the larger $C_p$ standard deviation observed at that TSR on figure 5 where it is expressed as error bars.

Figure 5 shows that for all onset flow velocities and all TSR values, there is little impact of the dummy tower proximity on the mean $C_p$ values. There is a notable exception at TSR = 2.5 when the onset flow velocity is $1\,\mathrm{m\,s^{-1}}$ , but this is believed to be due to the transition in flow regime as explained in the previous paragraph. Looking at the error bars of figure 5, there is however a noticeable effect of the dummy tower proximity on the standard deviation of $C_p$. This is most noticeable for the configuration where the dummy mast is the closest to the rotor, hinting towards increased fatigue on the structure due to cyclic loading.

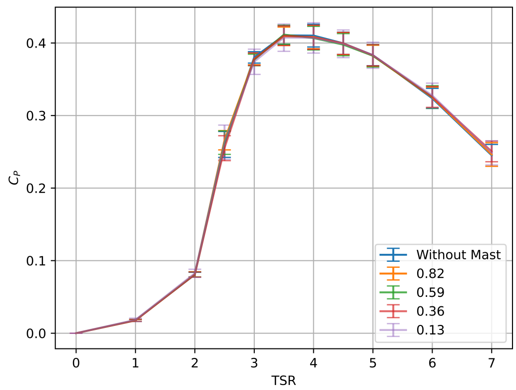


(a) TSR Sweep for Tidal Velocity $= 0.8m/s$

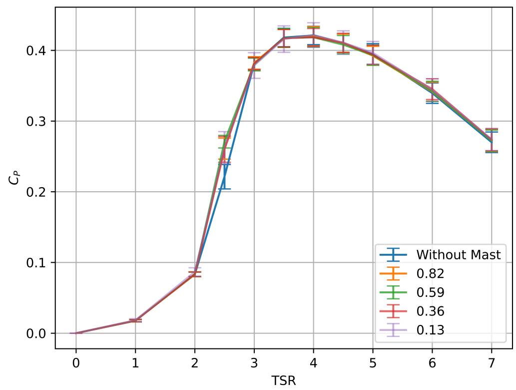


(b) TSR Sweep for Tidal Velocity $= 1.0m/s$

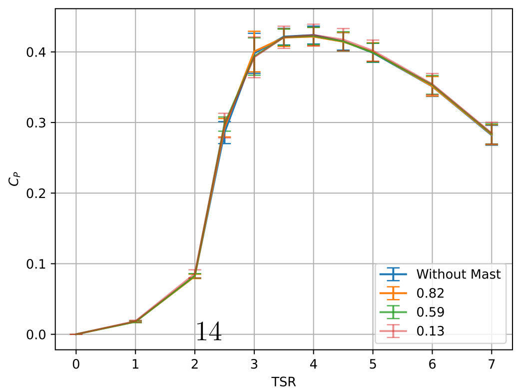




(c) TSR Sweep for Tidal Velocity $= 1.2m/s$

Figure 5: $C_p$ Curves for three onset flow velocities with four different normalised mast positions ($\hat{d}$) and a control experiment (without dummy mast) for reference. The error bars correspond to standard deviation.

A more in depth analysis of the standard deviation within $C_p$ and $C_t$ signals is carried out. The Coefficient of Variation (CoV) is obtained by normalising the standard deviation of the signal by its average value. The mathematical formulation for the CoV is given in equation 4.

$$CoV = \frac{\sigma}{\mu} \tag{4}$$

The CoV of the performance coefficients is plotted in figure 6 against $\hat{d}$. The onset flow velocity and the TSR for which the standard deviations are plotted are $1\,\mathrm{m\,s^{-1}}$ and 4 respectively.

We can notice that the CoV curve associated with $C_p$ is consistently above that of $C_t$. This is because of the normalisation by the mean associated with CoV computation and of the fact that at TSR = 4, mean $C_t$ is higher than mean $C_p$.

When the dummy tower is close to the rotor ($\hat{d} < 0.2$), there is a clear correlation between $C_p$ and $C_t$ CoVs and $\hat{d}$, with the CoVs decreasing as $\hat{d}$ increases. For $\hat{d} > 0.2$, the CoV values still exhibit some variations but these do not seem to be correlated with $\hat{d}$. To understand these variations better, we have plotted on the bottom graph of figure 6 the CoV of $U^2$ and $U^3$. $U^2$ and $U^3$ are respectively used in the computation of $C_t$ and $C_p$ to normalise the thrust (for $U^2$) and power (for $U^3$) as can be seen in equations 3 and 2. We can see that for $\hat{d} > 0.2$ the CoVs of the velocities exhibit variations with similar patterns as those observed for $C_p$ and $C_t$ CoVs, hinting at that the latter are caused by the velocity variations along the streamwise direction of the flume. In summary, for $\hat{d} < 0.2$, $C_p$ and $C_t$ CoVs are largely correlated with the position of the dummy tower but for $\hat{d} > 0.2$, they are caused by the variations in the onset flow velocity.

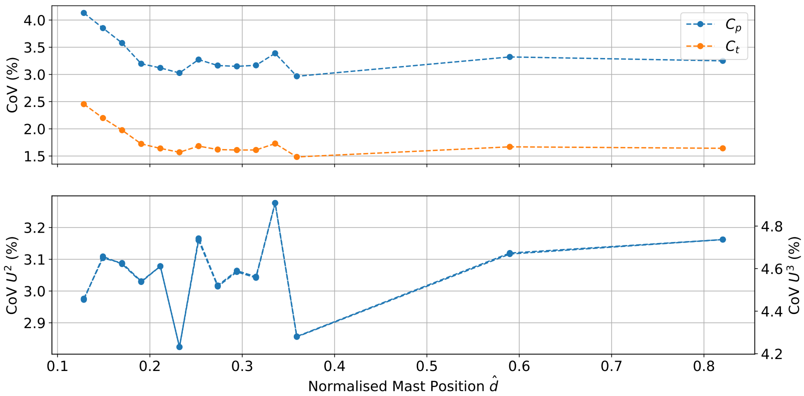


Figure 6: Variation in performance coefficients plotted against normalised distance from the rotor. The distance $\hat{d}$ between the dummy mast and the rotor plane are normalized by the rotor diameter. The turbine was tested at a flow velocity of $1\,\mathrm{m\,s^{-1}}$ and a TSR = 4. The variation in the square and cube of the velocity is plotted for comparison

### *4.2. Frequency-Domain Analysis*

The frequency domain analysis of the impact of the dummy tower proximity to the rotor on turbine loads focuses on the flapwise force on blade 1 ($F_{x_1}$), but similar results are observed for blade 2 and 3. Figure 7 shows the FFT (with log log axes) for $F_{x_1}$ at TSR = 4 and $U = 1\,\mathrm{m\,s^{-1}}$ for three increasing distances of the dummy mast to the rotor.

For the normalised frequency $f/f_0 < 0.4$, the spectra on the three subplots are very similar and are dominated by onset flow turbulence effects (as detailed in [18] and in [19]). For higher frequency values, the spectra are dominated by turbine related effects. On the top plot, the first seven clear peaks are labelled for convenience. The "1P" peak is associated to the passing of blade 1 in front of the dummy tower, which takes place once per rotor revolution, hence the associated normalised frequency of $f/f_0 = 1$. Given that the frequency of the "2P" peak is twice that of the "1P" peak and that its amplitude is lower than that of the "1P" peak, it is believed to be the first harmonic of the "1P" peak. The "3P" peak is higher than the "2P" peak and is therefore unlikely to correspond only to a harmonic of the "1P" peak. It is believed to be associated with the indirect effect of

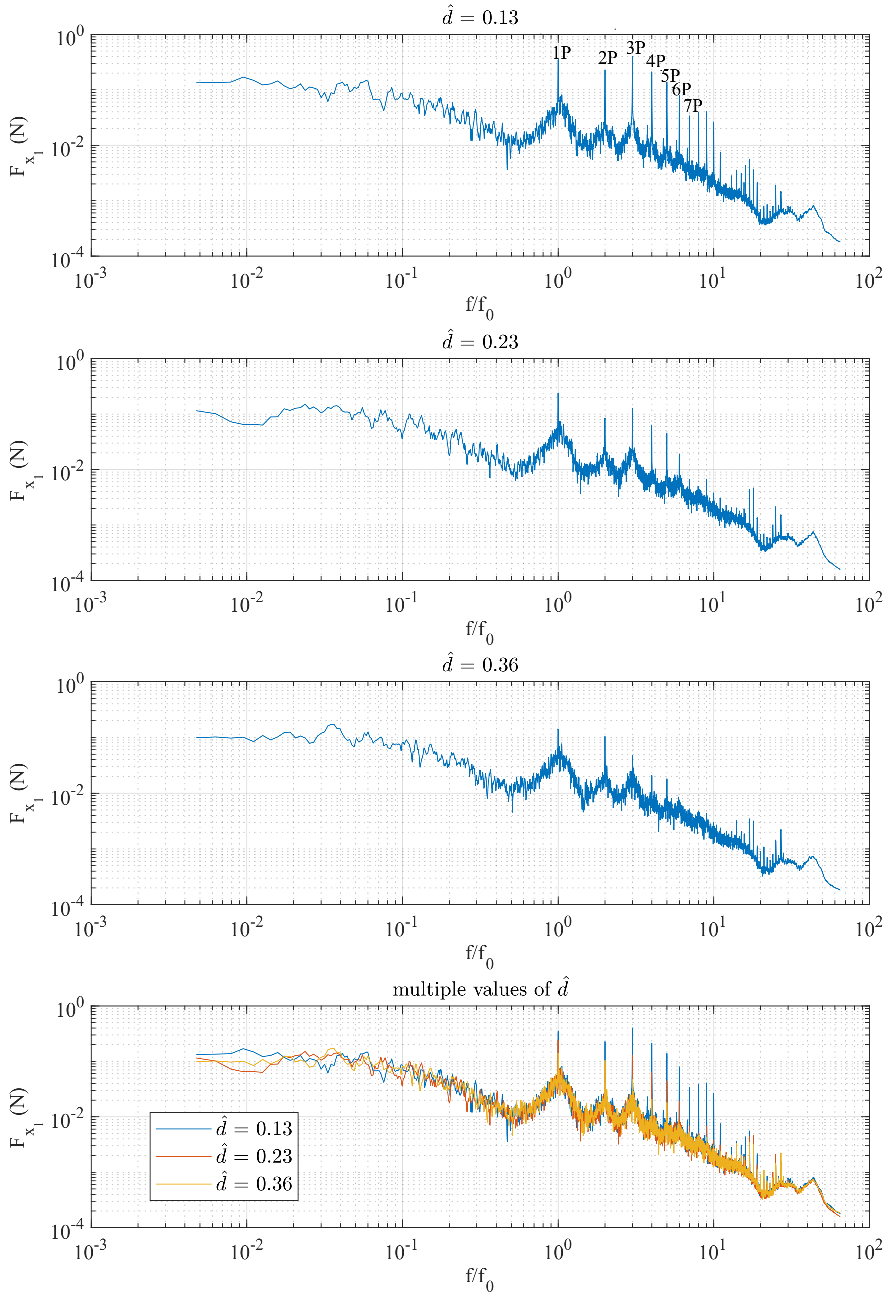




Figure 7: Frequency components amplitude (in Newtons) of the flapwise load on blade 1 ($F_{x_1}$) for increasing values of the distance between the rotor and the dummy mast ($\hat{d}$). Measurements were carried out at TSR = 4 and with an onset flow velocity $U = 1\,\mathrm{m\,s^{-1}}$. Both x and y axes are logarithmic and on the x-axis, the frequency is normalised by the rotational frequency $f_0$.

the passing of the three rotor blades in front of the dummy tower. Indeed, although those measurements are associated with only blade 1, it is likely that the loads induced on the rotor by the passing of the other blades in front of the dummy tower are felt to some extent by the sensor of blade 1, hence the higher value of the "3P" peak compared to the "2P" one. Given their frequency (multiples of those of the "1P" and "3P" peaks) and their decreasing amplitudes, the "4P" to "7P" peaks are believed to be harmonics of the the "1P" and "3P" peaks. Looking at those seven peaks on the different subplots, it can be seen that their amplitude decreases as the distance from the rotor to the dummy mast ($\hat{d}$) increases. This suggests a decreasing impact of the dummy tower on the $F_{x_1}$ loads at those specific frequencies, with increasing distance $\hat{d}$. It can be interpreted as a reduction of the tower shadowing effect with increased values of $\hat{d}$. Physically, the tower shadowing effect corresponds to a reduction in streamwise flow velocity upstream of the tower, due to the local blockage created by the tower. The further upstream of the tower, the less this velocity reduction phenomenon is pronounced. It should be noted that the amplitude values of the peaks displayed in figure 7 are not very accurate. Indeed, although those peaks are consisting of more than one point, they are still very narrow and their maximum values could therefore be affected by the smoothing technique used for plotting the FFTs. Indeed, in order to reduce noise on those plots, each point of the curves is derived through a moving average (in the frequency domain) with the width of the averaging window distributed logarithmically to match the log scale of the x-axis. In other words there is more averaging at high frequency than at low frequency. Nevertheless, we believe that the general qualitative trend of the peak amplitudes decreasing with increasing $\hat{d}$ is genuine. To quantify better this phenomenon, the amplitude of the two main peaks ("1P" and "3P") have been computed from raw FFT (i.e. without any smoothing) and plotted separately on figure 8 for all the values of $\hat{d}$ investigated.

It can be seen from figure 8 that the amplitudes of the "1P" and "3P" peaks generally decrease as $\hat{d}$ increases until $\hat{d} = 0.36$. For higher values of $\hat{d}$, the amplitude of the peaks remains broadly constant. The variability around the general trend of those curves is believed to be due to the difficulty in identifying the maximum value of those peaks. Indeed, although figure 8 was derived from non-smoothed FFT, given the narrowness of those peaks, it is likely that some amount of spillage is taking place in the FFT process, which distributes some of the amplitude of the main peak to the neighbour-

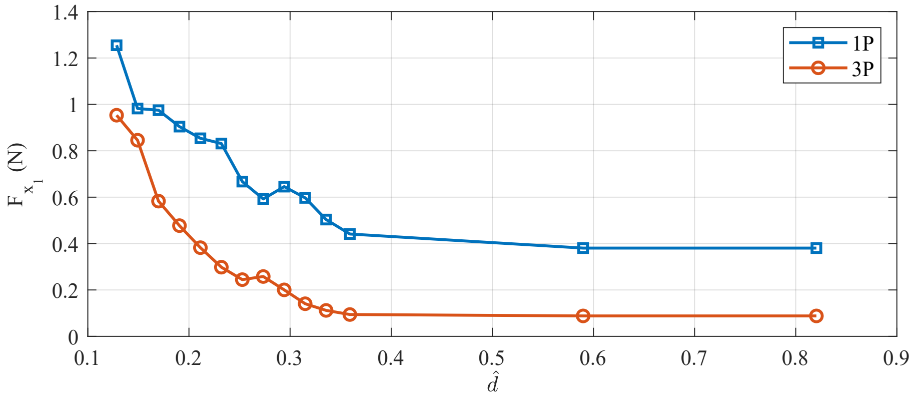


Figure 8: Amplitude (in Newton) of the "1P" and "3P" peaks of $F_{x_1}$ plotted against the normalised distance $\hat{d}$ between the rotor plane and the dummy tower axis.

ing frequencies. Nevertheless, figure 8 provides an indication of the impact of the distance between the rotor and the dummy mast on the influence of the latter on rotor loads. Ultimately, it also provides indications on the distance from which the dummy mast stops affecting those loads. Qualitatively, those results are consistent with what is observed in figure 6 for the coefficients of variation of $C_p$ and $C_t$. However, figure 8 shows a clear influence of the proximity of the dummy tower on the blade load for values of $\hat{d}$ up to 0.36 whereas from figure 6 this influence is not discernible for $\hat{d} > 0.23$. This suggests that the frequency analysis of a single blade flapwise load is more sensitive to the impact of the dummy tower presence on rotor loads than the coefficients of variation of $C_p$ and $C_t$ is.

On the top subplot of figure 7, it can be seen that there is a group of sharp peaks whose normalised frequency is $8 \leq f/f_0 \leq 11$. It is not entirely clear what those peaks are associated with. Their frequencies, which are integer multiples of those of the "1P" and/or "3P" peaks, suggests that they are harmonics of the "1P" and/or "3P" peaks. However the fact that the amplitudes of some of those peaks are higher than that of the "7P" peak is less consistent with that. It could however be that the amplitude of those high frequency peaks are not very reliable because of the smoothing technique and the potential spillage associated with the FFT process as explained earlier. In any case, the amplitudes of those peaks also decrease with increasing distance between the rotor and the dummy tower, thus suggesting that those peaks are somehow related to the influence of the dummy tower on the loads.

Finally, it can be noticed from figure 7 that aside from the sharp peaks discussed above, the general trend of the FFT curves are very similar regardless of the distance of the rotor to the dummy mast. This holds true even when the dummy mast is as far from the rotor as the structural mast ($\hat{d} = 0.82$) and in the absence of the dummy mast, as seen in figure 9. The figure shows the FFT of $F_{x_1}$ for the configuration with the dummy mast at its closest position to the rotor (blue curve), for the configuration where the dummy mast is in its farthest position from the rotor and aligned with the structural mast (red curve) and for the configuration without any dummy mast (yellow curve). Leaving aside the sharp peaks, the rest of the three curves are practically identical in trend. This suggests that the physical phenomena behind the three triangular peaks highlighted on the figure by dashed square boxes, are not associated with the presence of a tower. If they were, a difference in those broad peaks would be expected between the blue and red curves because of the significant difference in distance between the rotor and dummy tower between those two configurations. There would also be a difference in frequency of those broad peaks between the red and yellow curves. Indeed, the yellow curve is associated with a configuration with one tower whereas the red curve corresponds to a configuration with two identical towers, which are at the same distance from the rotor and 180° apart (with respect to the turbine rotor axis). In this latter configuration, the blade would experience a tower effect twice per revolution whereas in the former this would be once per revolution. Rather than being associated with the presence of the tower, those triangular peaks are believed to be caused by the rotational sampling effect of the onset flow by the rotating blades. In other words, the spectrum of the onset flow velocity, as measured from a fixed location (i.e. Eulerian measurement) is distorted when sampled from a point rotating along a circle, whose plan is perpendicular to the onset flow direction. One of the consequences of this distortion is the presence of narrow-banded peaks of turbulence energy centred on the frequency associated with the rotation and multiples of that frequency. This phenomenon was observed from experimental measurements and investigated in [34]. This has a direct impact on the load experienced by the blades, which are experiencing the onset flow through this rotational sampling effect. This phenomenon is derived semi-analytically for the turbine used in this study in [19].

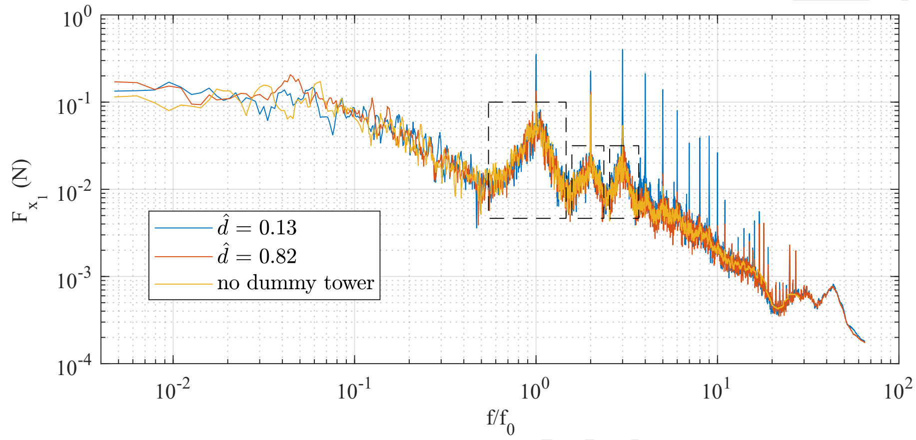


Figure 9: Frequency components amplitude (in Newtons) of the flapwise load on blade 1 ($F_{x_1}$) for the configurations corresponding to the closest position ($\hat{d} = 0.13$) of the dummy tower to the rotor (blue curve), the configuration with furthest dummy tower position ($\hat{d} = 0.82$, red curve) and the configuration without dummy tower (yellow curve). Measurements were carried out at TSR = 4 and with an onset flow velocity $U = 1\,\mathrm{m\,s^{-1}}$. Both x and y axes are logarithmic and on the x-axis, the frequency is normalised by the rotational frequency $f_0$.

### *4.3. Azimuthal Variation of the loads*

An interesting way to investigate the impact of the proximity of the dummy mast onto rotor loads is to analyse those loads as a function of the absolutes azimuthal position of the rotor. To do so, starting from synchronised timeseries of load measurements and absolute azimuthal positions, the load values are binned according to their associated angular position, with an angular bin width of 1°. Load values are then averaged on a bin by bin basis so that the final outcome is one load value per degree of azimuthal position of the rotor.

Figure 10 shows the azimuthal analysis, in the form of polar plots, for the rotor torque and for different distances of the dummy mast to the rotor plan. These measurements are associated with an onset flow velocity of $1\,\mathrm{m\,s^{-1}}$ and TSR = 4.

Looking at the polar plot corresponding to $\hat{d} = 0.13$, we observe two main features.

The first one is the "clove-like pattern" with three "leaves" or lobes. Between those lobes, there are well defined notches which are 120° apart, with one of them at 0°. Those notches are believed to be due to the dummy tower shadowing effect which is experienced by the rotor three times per revolution i.e. each time a blade passes the dummy tower. Indeed, upstream of the dummy tower, the flow velocity is locally reduced, which in turn reduces the load experienced by the blades when they pass through that region of the flow. The notch at 0° is consistent with the fact that that angle corresponds to the top dead centre position for blade 1, i.e. when it is aligned with the dummy tower. The 120° gap between the notches is also consistent with the angular spacing between the blades of the rotor. It is interesting to note that the amplitude of the notches decreases as the distance from the rotor to the dummy mast increases, highlighting the diminishing impact of the tower on the rotor torque oscillations as the dummy mast is located further away from the rotor plane.

The second clear feature is the ripple like pattern of smaller amplitude than that of the "clove -like" one but which exhibits 18 oscillations per revolution. Those oscillations do not seem to be associated with the proximity of the dummy tower as their amplitude, frequency and phase remain largely unaffected by the dummy tower position. Moreover, observations for other TSRs (not shown in figure 10) yield a similar pattern. All this suggests that this feature is not related to any hydrodynamic phenomena but to a mechanical artefact of the drivetrain, possibly due to cogging in the turbine motor or gearbox.

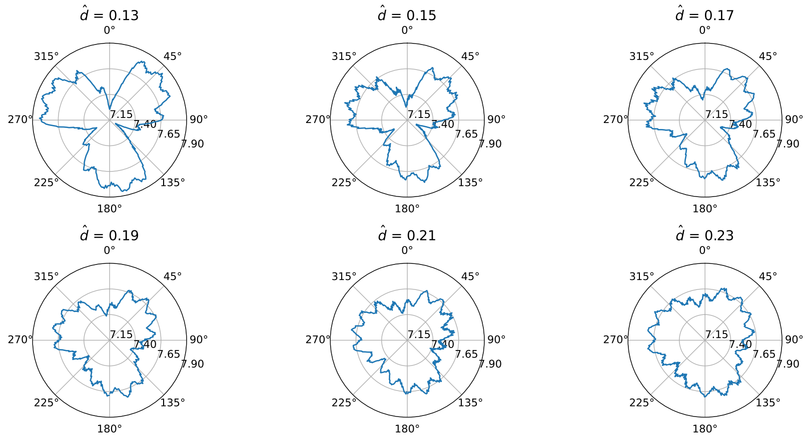


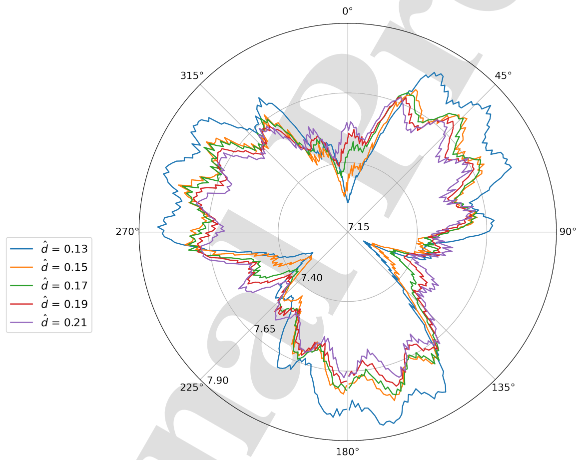


Figure 10: Angle averaged rotor torque (in N m) plotted against the absolute rotor angular position for six different dummy mast positions. 0° corresponds to when blade 1 is at top dead centre. This data corresponds to TSR = 4 and to an onset flow velocity of $1\,\mathrm{m\,s^{-1}}$ . The second image combines the six individual plots to provide a comparitive view point.

Figure 11 shows the azimuthal analysis for the flapwise force for blade 1 for different values of the normalise distance between the dummy tower and the rotor plane.

The main feature of the curve for $\hat{d} = 0.13$ is a notch at 0°. This is once again believed to be associated with the presence of the dummy tower. Unlike for figure 10, there is only one notch here because the measurements are associated with only one blade, which therefore experiences the flow deceleration associated with the dummy tower only once per rotor revolution. The lobes on each side of the notch are not symmetrical, with the one at 45° being larger than the one at 315°. This lack of symmetry is believed to be due to the rotational direction of the turbine. In other words, if the turbine was to rotate in the other direction, the lobes pattern would be reversed. We notice that the notch and lobes pattern is less pronounced as $\hat{d}$ increases. As for figure 10, this is believed to be due to the decreasing influence of the tower on the loads with the increasing distance between the rotor and the tower. Finally, we notice that the angular position of the notch drifts progressively as $\hat{d}$ increases, from 0° for $\hat{d} = 0.13$ to reach about 350° for $\hat{d} = 0.23$. This angular drift is believed to be associated with the swirl in the rotor wake, induced by the turbine rotation. The local flow deceleration in the streamwise direction upstream of the tower is shifted in the rotor tangential direction by the swirl. The larger the distance between the rotor and the tower, the longer the "swirl effect" applies to the tower deceleration and therefore the larger the angular shift observed. As for the asymmetry in the lobes pattern, it is believed that if the turbine was to be spinning in the other direction, the angular drift of the notch position with $\hat{d}$ would be in the opposite direction to what is observed in the figure 11 as the swirl would be rotating in the other direction.

To provide some perspective on the magnitude of those tower induced loads, they can be compared with loads associated with turbulence and wave. From figure 11, it can be seen that the difference between the minimum and maximum force values is about 10 N for the shortest distance $\hat{d} = 0.13$. This difference gradually decreases when $\hat{d}$ increases, from 8 N at $\hat{d} = 0.15$ to 2 N at $\hat{d} = 0.23$. In [13] and [14] the exact same turbine model is used in the same flume to investigate blade loads induced by strong shear flow effects. These studies show that the flapwise force on blade 1 records azimuthal-averaged variations of between 3 N and 12 N, depending on the turbine position in the shear flow, for the same onset flow velocity as for figure 11. That is the same order of magnitude as the $F_{x_1}$ fluctuations observed in the present study. In [35], a section is dedicated to the variation of blade root bending moments for a turbine model subjected to a combination of irregular wave and shear flow conditions, in the same tank as the present study. The turbine experiences azimuthal-averaged variations of the out-of-plan blade root bending moment of between 3 N m and 5 N m, depending of the depth of the turbine. This turbine is slightly larger than the one used in the present study, with a rotor diameter of 0.9 m. From the measurements provided in [35] we can make a rough estimation of the blade flapwise force azimuthal variation, based on the assumption that the point of application of the force on the blade is located at 75% of the blade span. This yields a range of 8 N to 14 N, corresponding to the same order of magnitude as the variations recorded in this study, for shorter blades.

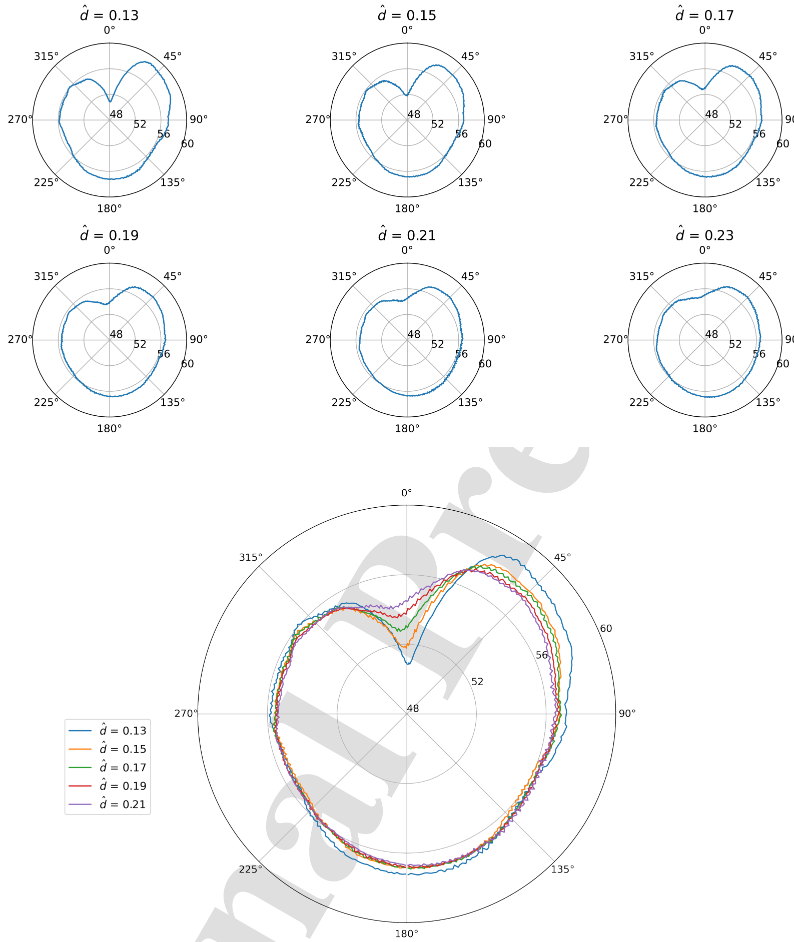


Figure 11: Angle averaged flapwise force on blade 1 (in N) plotted against the absolute rotor angular position for six different dummy mast positions. 0° corresponds to when blade 1 is at top dead centre. Those data corresponds to TSR = 4 and to an onset flow velocity of $1\,\mathrm{m\,s^{-1}}$ . The second image combines the six individual plots to provide a comparitive view point.

### 4.4. *Exceedence analysis*

The highest loads experienced by tidal turbine components and their probability of occurrence are key information for their engineering design. In order to illustrate how these high loads and their distribution is affected by the proximity of the tower to the rotor, we have plotted in figure 12 the exceedance probability of the flapwise force on blade 1, for different positions of the dummy tower. The exceedance probability is a statistical quantity providing information on the probability that a certain value (in our case of flapwise force on blade 1) is met or exceeded. The curves of figure 12 were obtained by sorting the load timeseries in ascending order in terms of load measurements with the probability of exceedance associated with each load value being calculated by dividing the index of that measurement (after sorting) by the total number of measurement points. More information on the concept of exceedance probability can be found in [36]. On the x-axis, $F_{x_1}$ is normalised by its mean value. Those curves were obtained for tests at TSR = 4 and onset flow velocity of $1\,\mathrm{m\,s^{-1}}$. Each curve corresponds to a test run of 4200 s. The runtime for the tests was set to be significantly longer than for the other tests of the study in order to increase statistical robustness.

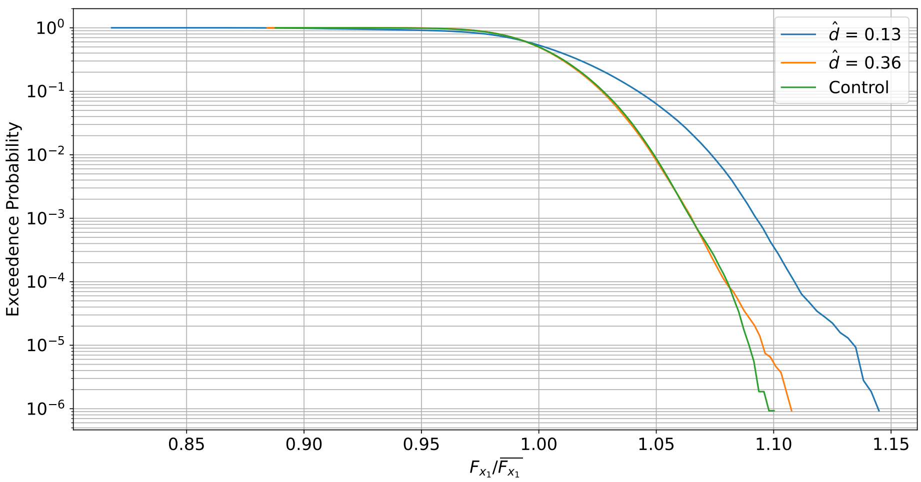


Figure 12: Exceedance probability of the flapwise force on blade 1 ($F_{x_1}$) for different dummy tower positions within onset flow velocity of $1\,\mathrm{m\,s^{-1}}$ and TSR = 4.

The blue curve is associated with a normalised tower distance to the rotor

$\hat{d}$ of 0.13 and orange one to a distance of 0.36. The green one corresponds to the configuration without any dummy tower. The three curves largely overlap for $F_{x_1}/\bar{F_{x_1}} < 1$ but beyond that point, there is a clear pattern of higher load for a given probability and higher probability for a given load for the $\hat{d} = 0.13$ curve compared with the two others. For exeedance probability values higher than $10^{-4}$, the $\hat{d} = 0.36$ curve and the one corresponding to the configuration without dummy tower overlap. This means that at that distance ($\hat{d} = 0.36$), the dummy tower has little effect on the load probability distribution over $10^{-4}$. For exeedance probability value lower than $10^{-4}$, the loads are higher for the orange curve compared to the green one, which is consistent the "higher load with lower $\hat{d}$" pattern observed throughout the study. It should however be noted that the low exceedance probability tails of the curves are less smooth than for higher probability exeedance values. This is due to the fact that in those low probability regions, the curves are often defined by a limited number of data points. This is actually not very statistically robust and the very tail of those curves should therefore be considered with caution. Nevertheless, figure 12 highlights the fact that the tower distance to the rotor should be taken into account for blade components maximum load considerations.

## 5. Conclusions

This study has investigated experimentally the impact of the proximity of the tower to the rotor on turbine performance and structural loads. This was achieved using a dummy tower whose position was accurately controlled. Tests were carried out for different onset flow velocities and different distances from the rotor plane to the dummy tower axis.

The results show that there is little impact of the distance between the rotor and the dummy tower on the mean values of the $C_p$ and $C_t$ coefficients. This is in contrast with the findings reported in [30] where CFD computations predicts higher values of mean $C_p$ and $C_t$ with increasing values of $\hat{d}$. The discrepancy could be explained by the fact that the diameter of the mast considered in the CFD study is significantly larger than in our study (24% of the rotor diameter for [30] versus 10.3% for our study). Moreover, in [30], the mast extends through the full height of the water column whereas in our study, it only extends from the nacelle to the water surface, which represents half of the water column height.

Going back to the $C_p$ and $C_t$ values measured in this study, variations in those two coefficients are clearly impacted by that distance, with their respective coefficient of variation being higher when the dummy tower is closer to the rotor. For $\hat{d} > 0.23$, the influence of the dummy tower is no longer discernible.

Results were also examined in terms of frequency analysis, focusing on the flapwise load on one of the blades. In that context, the impact of the proximity of the dummy tower to the rotor is exhibited by very sharp and narrow peaks at the blade passing frequency and its harmonics. The amplitude of those peaks decreases with increasing values of $\hat{d}$. The frequency analysis suggests that the impact of the dummy tower on $F_{x_1}$ is noticeable for values of the up to 0.36, which is more than what was observed for the coefficient of variation of $C_p$ and $C_t$. This difference is believed to be due to the fact that the frequency analysis is more sensitive. The frequency analysis also highlights the two components of the peaks taking place at the blade passing frequency and its harmonics; with one due to the proximity of the dummy tower and the other associated with the rotational sampling effect. The former is very narrow and its amplitude decreases as the distance between the dummy tower and the rotor increases whereas the latter is broader and unrelated to the dummy tower position.

The azimuthal analysis also clearly highlights the diminishing impact of the dummy tower with the increasing distance from the rotor to the dummy mast. It also exhibits how the swirl in the rotor wake shifts the azimuthal angle at which tower shadowing effect is "felt" by the rotor with increasing $\hat{d}$. Comparisons with other studies using the same or a similar turbine model shows that the recorded azimuthal variations of the flapwise force are of the same order of magnitude as the ones caused by wave and shear flow effects, especially for the shortest values of $\hat{d}$.

Flapwise loads on one of the blades are investigated with a load exeedance probability analysis. This simple exeedance analysis is not a substitute for an in-depth extreme value analysis, which is beyond the scope of this study, but it nevertheless provides valuable insight in the distributions of the loads and their probability. This analysis shows that when the dummy tower is close to the rotor, it significantly increases the value of the highest loads experienced by the blade, compared with the when the dummy mast is further away. This exeedance probability analysis requires long timeseries (4200 s in this study) and it was therefore not practical to carry out such long tests for a large number of values of $\hat{d}$. As a consequence, we cannot see the gradual evolution of the exeedance curves with $\hat{d}$ but only that for $\hat{d} = 0.36$, the exeedance curve is very similar to that associated with the configuration without dummy mast, except for the lowest probability region in which the tail of the curves is less reliable.

Overall, this study shows that the proximity of the turbine tower to the rotor has little influence on mean values of performance and load coefficients but has a clear impact on load and performance variations as well as on maximum load values. The general trend is that the closer the tower is to the rotor the higher those variations and maximum values are. This suggests that the distance between the tower and the rotor should be taken into account at turbine design stage. Further studies could involve investigating experimentally how the diameter and the section geometry of the mast affect rotor loading. It would also be interesting to compare experimentally rotor loading for the same dummy mast located upstream and downstream of the rotor. Finally, it would be useful expand this type of experiments to higher Reynolds numbers to investigate the Reynolds dependency of the value of $\hat{d}$ above which the mast has no significant impact on rotor loads.

## CRediT authorship contribution statement

**Gohar Shoukat:** Conceptualisation, Methodology, Formal analysis, Writing - original draft, Visualisation. **Benoît Gaurier:** Conceptualisation, Methodology, Formal analysis, Writing - review and editing. **Jean-Valéry Facq:** Resource, Visualisation. **Grégory S. Payne:** Conceptualisation, Methodology, Formal analysis, Writing - original draft, Writing - review and editing, Visualisation, Supervision, Project administration, Funding.

## Declaration of competing interest

The authors declare that they have no known competing financial interests or personal relationships that could have appeared to influence the work reported in this paper.

## Acknowledgements

This work was conducted as part of the French THeoREM Infrastructure research programme. The authors would like to thank Dr Grégory Germain from IFREMER for his assistance with the funding application. We would also like to thank Thomas Bacchetti from IFREMER for his assistance with the experimental work. Finally, Payne G.S. would like to thank Dr Georgios Deskos from NREL, Prof Sandrine Aubrun and Dr Jean-Christophe Gilloteaux from Ecole Centrale de Nantes for their very useful discussions on the topics of rotational sampling effect and tower shadowing effect.

## References

[1] Ocean energy strategic roadmap. Building ocean energy for Europe, https://webgate.ec.europa.eu/maritimeforum/sites/default/files/OceanEnergyForum_Roadmap_Online_Version_08Nov2016.pdf.

[2] Orbital marine power, latest news 2021, https://orbitalmarine.com/news/.

[3] S. G. Parkinson, W. J. Collier, Model validation of hydrodynamic loads and performance of a full-scale tidal turbine using tidal bladed, International Journal of Marine Energy 16 (2016) 279–297. doi:doi.org/10.1016/j.ijome.2016.08.001.

[4] Meygen tidal energy project phase 1a, https://simecatlantis.com/projects/meygen/.

[5] D. Magagna, R. Monfardini, A. Uihlein, JRC Ocean Energy Status Report: 2016 Edition, Scientific analysis or review, Policy assessment KJ-1A-28407-EN-N (online), Luxembourg (2016). doi:10.2760/509876.

[6] D. Magagna, A. Uihlein, Ocean energy development in Europe: Current status and future perspectives, International Journal of Marine Energy 11 (2015) 84–104. doi:10.1016/j.ijome.2015.05.001.

[7] J. L. Villate, P. Ruiz-Minguela, J. Berque, L. Pirttimaa, D. Cagney, C. Cochrane, H. Jeffrey, Strategic Research and Innovation Agenda for Ocean Energy (2020).

URL https://www.oceanenergy-europe.eu/wp-content/uploads/2020/05/ETIP-Ocean-SRIA.pdf

[8] T. Corsatea, D. Magagna, Overview of european innovation activities in marine energy technology, Policy assessment LD-NA-26724-EN-N (online), Luxembourg (2014). doi:10.2790/29334.

[9] A. Vinod, C. Han, A. Banerjee, Tidal turbine performance and near-wake characteristics in a sheared turbulent inflow, Renewable Energy 175 (2021) 840–852. doi:10.1016/j.renene.2021.05.026.

[10] A. Vinod, A. Banerjee, Performance and near-wake characterization of a tidal current turbine in elevated levels of free stream turbulence, Applied Energy 254 (April) (2019) 113639. doi:10.1016/j.apenergy.2019.113639.

[11] M. Thiébaut, J. F. Filipot, C. Maisondieu, G. Damblans, R. Duarte, E. Droniou, N. Chaplain, S. Guillou, A comprehensive assessment of turbulence at a tidal-stream energy site influenced by wind-generated ocean waves, Energy 191 (2020). doi:10.1016/j.energy.2019.116550.

[12] L. Furgerot, A. Sentchev, P. Bailly Du Bois, G. Lopez, M. Morillon, E. Poizot, Y. Méar, A. C. Bennis, One year of measurements in Alderney Race: Preliminary results from database analysis: In situ measurements in Alderney Race, Philosophical Transactions of the Royal Society A: Mathematical, Physical and Engineering Sciences 378 (2178) (2020). doi:10.1098/rsta.2019.0625.

[13] B. Gaurier, P. Druault, M. Ikhennicheu, G. Germain, Experimental analysis of the shear flow effect on tidal turbine blade root force from three-dimensional mean flow reconstruction, Philosophical Transactions of the Royal Society A: Mathematical, Physical and Engineering Sciences 378 (2178) (2020). doi:10.1098/rsta.2020.0001.

[14] B. Gaurier, M. Ikhennicheu, G. Germain, P. Druault, Experimental study of bathymetry generated turbulence on tidal turbine behaviour, Renewable Energy 156 (2020) 1158–1170. doi:10.1016/j.renene.2020.04.102.

[15] E. Fernandez-Rodriguez, T. Stallard, P. K. Stansby, Experimental study of extreme thrust on a tidal stream rotor due to turbulent flow and with

opposing waves, Journal of Fluids and Structures 51 (2014) 354–361. doi:10.1016/j.jfluidstructs.2014.09.012.

[16] I. A. Milne, A. H. Day, R. N. Sharma, R. G. Flay, The characterisation of the hydrodynamic loads on tidal turbines due to turbulence, Renewable and Sustainable Energy Reviews 56 (2016) 851–864. doi:10.1016/j.rser.2015.11.095.

[17] L. P. Chamorro, C. Hill, S. Morton, C. Ellis, R. E. A. Arndt, F. Sotiropoulos, On the interaction between a turbulent open channel flow and an axial-flow turbine, Journal of Fluid Mechanics 716 (2013) 658–670. doi:10.1017/jfm.2012.571.

[18] G. S. Payne, T. Stallard, R. Martinez, T. Bruce, Variation of loads on a three-bladed horizontal axis tidal turbine with frequency and blade position, Journal of Fluids and Structures 83 (2018) 156–170. doi:10.1016/j.jfluidstructs.2018.08.010.

[19] G. Deskos, G. S. Payne, B. Gaurier, M. Graham, On the spectral behaviour of the turbulence-driven power fluctuations of horizontal-axis turbines, Journal of Fluid Mechanics 904 (2020). doi:10.1017/jfm.2020.681.

[20] T. Blackmore, L. E. Myers, A. S. Bahaj, Effects of turbulence on tidal turbines: Implications to performance, blade loads, and condition monitoring, International Journal of Marine Energy 14 (2016) 1–26. doi:10.1016/j.ijome.2016.04.017.

[21] A. Bahaj, A. Molland, J. Chaplin, W. Batten, Power and thrust measurements of marine current turbines under various hydrodynamic flow conditions in a cavitation tunnel and a towing tank, Renewable Energy 32 (3) (2007) 407–426. doi:10.1016/j.renene.2006.01.012.

[22] C. Frost, I. Benson, P. Jeffcoate, B. Elsäßer, T. Whittaker, The effect of control strategy on tidal stream turbine performance in laboratory and field experiments, Energies 11 (6) (2018). doi:10.3390/en11061533.

[23] A. Nambiar, S. Draycott, G. S. Payne, B. Sellar, A. Kiprakis, Influence of tidal turbine control on performance and loads, Applied Ocean Research 114 (June) (2021) 102806. doi:10.1016/j.apor.2021.102806.

[24] K. Van Ness, C. Hill, J. Burnett, A. Aliseda, B. Polagye, Experimental comparison of blade pitch and speed control strategies for horizontal-axis current turbines, Journal of Ocean Engineering and Marine Energy 7 (1) (2021) 83–96. doi:10.1007/s40722-021-00188-w.

[25] U. Ahmed, D. Apsley, I. Afgan, T. Stallard, P. Stansby, Fluctuating loads on a tidal turbine due to velocity shear and turbulence: Comparison of cfd with field data, Renewable Energy 112 (2017) 235–246. doi:10.1016/j.renene.2017.05.048.

[26] W. Finnegan, E. Fagan, T. Flanagan, A. Doyle, J. Goggins, Operational fatigue loading on tidal turbine blades using computational fluid dynamics, Renewable Energy 152 (2020) 430–440. doi:https://doi.org/10.1016/j.renene.2019.12.154.

[27] J. Thé, H. Yu, A critical review on the simulations of wind turbine aerodynamics focusing on hybrid rans-les methods, Energy 138 (2017) 257–289. doi:10.1016/j.energy.2017.07.028.

[28] S. Muchala, R. H. Willden, Influence of support structures on tidal turbine power output, Journal of Fluids and Structures 83 (2018) 27–39. doi:10.1016/j.jfluidstructs.2018.08.008.

[29] A. Mason-Jones, D. M. O'Doherty, C. E. Morris, T. O'Doherty, Influence of a velocity profile  support structure on tidal stream turbine performance, Renewable Energy 52 (2013) 23–30. doi:10.1016/j.renene.2012.10.022.

[30] C. Frost, C. E. Morris, A. Mason-Jones, D. M. O'Doherty, T. O'Doherty, The effect of tidal flow directionality on tidal turbine performance characteristics, Renewable Energy 78 (2015) 609–620. doi:10.1016/j.renene.2015.01.053.

[31] B. Gaurier, G. Germain, J. Facq, Experimental study of the Marine Current Turbine behaviour submitted to macro-particle impacts, in: Proceedings of the 12th European Wave and Tidal Energy Conference, Cork, Ireland, 2017.

[32] G. Germain, Marine current energy converter tank testing practices, in: 2nd International Conference on Ocean Energy, Brest, France, 2008. URL https://archimer.ifremer.fr/doc/00022/13366/

[33] B. Gaurier, G. Germain, J.-V. Facq, T. Bacchetti, Wave and current flume tank of IFREMER at Boulogne-sur-mer. Description of the facility and its equipment, Report 19CSMBL18 (2018). doi:10.13155/58163.

[34] J. R. Connell, THE SPECTRUM OF WIND SPEED FLUCTUATIONS ENCOUNTERED BY A ROTATING BLADE OF A WIND ENERGY CONVERSION SYSTEM, Solar Energy 29 (5) (1982) 363–375. doi:doi.org/10.1016/0038-092X(82)90072-X.

[35] M. Allmark, R. Martinez, S. Ordonez-Sanchez, C. Lloyd, T. O'doherty, G. Germain, B. Gaurier, C. Johnstone, A phenomenological study of lab-scale tidal turbine loading under combined irregular wave and shear flow conditions, Journal of Marine Science and Engineering 9 (6) (2021). doi:10.3390/jmse9060593.

[36] A. C. McMahan, C. N. Grover, F. E. Vignola, Chapter 4 - Evaluation of Resource Risk in Solar-Project Financing, in: J. Kleissl (Ed.), Solar Energy Forecasting and Resource Assessment, Academic Press, Boston, 2013, pp. 81–95. doi:doi.org/10.1016/B978-0-12-397177-7.00004-8.

Gohar Shoukat - Conceptualisation, Methodology, Formal analysis, Writing - original draft, Visualisation.

Benoît Gaurier - Conceptualisation, Methodology, Formal analysis, Writing - review and editing.

Jean-Valéry Facq - Resource, Visualisation.

Grégory S. Payne - Conceptualisation, Methodology, Formal analysis, Writing - original draft, Writing - review and editing, Visualisation, Supervision, Project administration, Funding.

**Declaration of interests**

☒ The authors declare that they have no known competing financial interests or personal relationships that could have appeared to influence the work reported in this paper.

☐ The authors declare the following financial interests/personal relationships which may be considered as potential competing interests: